Experimental report – MD1375

Beamline: ID19

Users:
Ludovic Broche (ESRF - Beamline ID19) ; Guillaume Brotons (IMMM, CNRS UMR 6283) ;
Isabelle Morfin (ESRF - Beamline D2AM) ; Alexandra Pierron (IMMM, CNRS UMR 6283)

PART A. Scientific background

Our research topic is based on the study of a new generation of synthetic bone for substitution and regenerative therapy for patients suffering from mandibular osteoradionecrosis (ORM). This pathology is due to a major complication of cancers of the upper aerodigestive tract after treatment with radiotherapy. It is characterized by soft tissue and bone necrosis and can lead to pathological fractures often associated with significant bacterial infection. In the case of small defects, the bones are able to regenerate, but for critical-size defects, major surgical interventions must be considered, such as autologous bone grafting. However, this type of procedure has its drawbacks and can result in high donor site morbidity. In recent years, alternative solutions have emerged with the development of tissue engineering technology. Synthetic biomaterials mimicking bone behavior and promoting osteogenesis are particularly studied.

As such, our technology consists in the elaboration of a new hybrid nanocomposite via a bricks-and-mortar approach, with bioactive glass nanoparticles (SiO_2-CaO-P_2O_5 bricks), functionalized with customized polymers (PDLLA, poly (lactic acid) mortar). The synthetic bone grafts, or "scaffolds", are obtained by freeze-casting a dimethyl carbonate (DMC) solution containing the aforementioned silica-based nanoparticles and the PLA derivates. This Temperature-Induced Phase Separation (TIPS) applies a temperature gradient to the solution allowing crystals of solvent to grow in one specific direction. The solidified medium is then lyophilized leading to a hierarchical porous material, referred to as "scaffold", offering the microporosities necessary for their colonization by biological tissues after implantation as well as for the mechanical properties of the material.

To understand the scaffolds' structure and mechanical properties, as brittleness impairs their cut by the surgeon and their fate *in-vivo*, a three-part experiment was conducted using 3D X-ray imaging techniques at ESRF-ID19 (April 2023-MD1375): 1) Static multi-resolution phase contrast tomography to characterize both the macro-structure and the particle density over the material on scaffolds designed prior to the experiment (the substrate used during freeze-casting being mirror-polished copper caps); 2) Fast-phase contrast tomography *in-operando* freeze-casting experiments by cooling the solid/solution interface using a dedicated X-ray tomography users-sample environment (the substrate used in that case being polished aluminum caps); 3) *In-situ* phase-contrast tomography of mechanically compress scaffold samples using the TomoPress at ID19.

The data analyses were conducted using Image J (Fiji) and Blender as well as other commercial softwares such as Dragonfly, Imorph and VG Studio max.

The following experimental report aims to present the main results obtained from the data reconstruction and analysis of the three-part assessment mentioned above. For this first ID19 synchrotron experiment, our aim was more to carry out proof-of-concept experiments than to measure a large number of samples (1- High-resolution on finalized scaffolds; 2- i*n-situ* freeze-casting experiments and 3- compression experiments).

PART B. 1) High Resolution Tomography and 2) *In-situ* freeze-casting Tomography

B.1) Static multi-resolution phase contrast tomography allowed the characterization of the micro- and macrostructure over the cm^3 sample volume. The low resolution (3.1 µm) gave us an almost complete view of the sample (8x8x7 mm^3), while the high resolution (0.65 µm) displayed a partial view of the volume (1.7x1.7x1.4 mm^3) but gave us access to finer geometry measurements. In this way, a multiscale porosity was depicted (**Figure 1**):

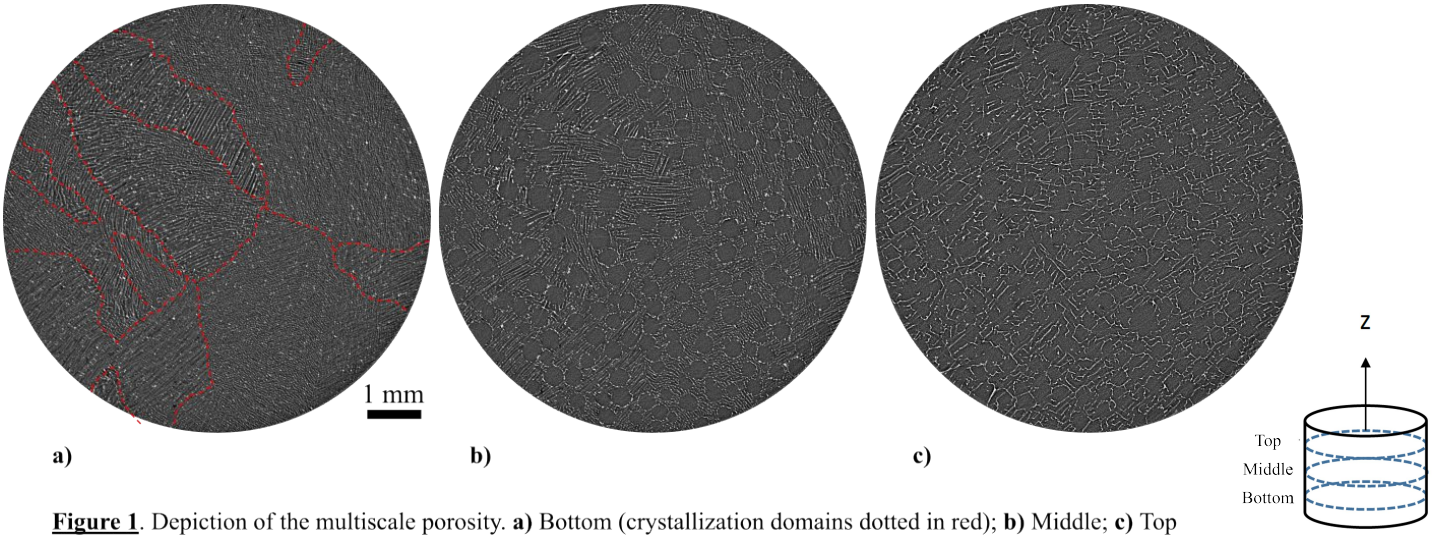

Figure 1. Depiction of the multiscale porosity. **a)** Bottom (crystallization domains dotted in red); **b)** Middle; **c)** Top
Sample considered: Scaffold with non-grafted and non-functionalized binary nanoparticles (SiO_2-CaO, $d \sim 164\ nm$), $T_{FC} = -10°C$, Ratio Polymer/Np 51/49, Low resolution

i) An expected ladder-like microporosity between the nano-brick walls formed during the scaffold's freeze-casting due to the expulsion of the nanoparticles by the solvent crystallites.

ii) A macroporosity in the form of cylindrical tubes, often starting near the cold plate at the bottom of the freeze-casting sample chamber (solid/liquid interface) and reaching the surface of the sample in some cases (air/liquid interface).

Looking first at a scaffold made with non-grafted and non-functionalized binary nanoparticles (SiO_2-CaO, $d \sim 164\ nm$), a freeze-casting temperature of $-10°C$ and a free polymer/nanoparticles ratio of 51/49, we observe that the ladder-like microporosities are dense at its bottom ($d_{\mu pores,bottom} \sim 31 \mu m$) and get wider towards the top ($d_{\mu pores,top} \sim 94\ \mu m$). A similar behavior is observed for the macropores which are not quite discernable at the bottom but appear rapidly going up ($d_{Mpores,bottom} \sim 186\ \mu m$; $d_{Mpores,top} \sim 415\ \mu m$). As we approach the top of the scaffold, we lose the clear distinction of the circular shape of the macropores as the micropores grow larger and the two pore types tend to merge.

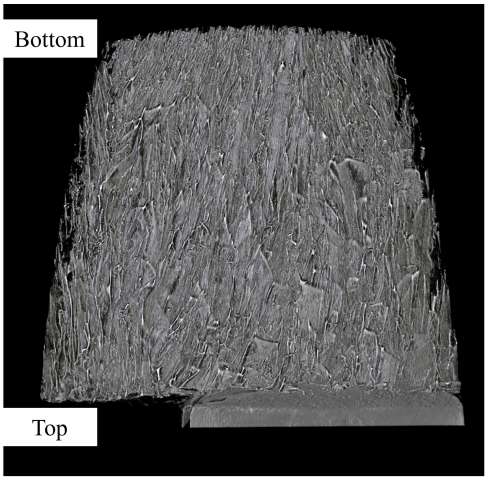

Figure 2. Porous scaffold volume rendering

Furthermore, although the general direction of the walls and the pores within the scaffold is vertical, a 3D volume rendering reveals many wall orientations (**Figure 2**). Looking at the slice closest to the cold bottom plate, we observe several crystallization

domains (**Figure 1.a**). This phenomenon could be explained by the surface condition of the substrate used during crystallization, as the domains seem to follow patterns typical of the "facets" of the metallic substrate.

It should also be pointed out that the difference in pore size, depending on the slice considered, can contribute to varying stress levels on the walls, therefore guiding their orientation. Additionally, focusing on the side of the scaffold, the images show what appears to be a direction of crystal propagation coming from the edges. These results suggest that the substrate surface and the sample chamber envelope offer different preferential nucleation zones.

Note that high resolution images show large clusters of dots on sections at the bottom of the scaffold, which could be attributed to the tendency of the nanoparticles to sediment in the solvent at the start of crystallization.

The comparison with a scaffold made with grafted and functionalized nanoparticles does not show much difference with the results presented above apart from the distinction of a crevice in a semi-circle at the bottom of the scaffold. Similar to the behavior of the micro- and macropores, this crevice grows bigger towards the top ($width_{crevice,bottom} \sim 101\ \mu m$; $width_{crevice,top} \sim 407\ \mu m$). Its presence could be explained by the varying patterns of roughness of the substrate surface. It therefore shows the importance of the aformentioned surface considering that the crevice covers the entire height of the scaffold. Now compared to a scaffold made with quaternary nanoparticles this time (SiO_2-CaO-P_2O_5, doped with copper oxides, $d \in [400\ nm - 10\ \mu m]$) and a different polymer/Np ratio (90/10), the only apparent difference appears to be the walls' thickness (approx. 36% thicker). This could be explained by the larger size of the nanoparticles and their greater steric hindrance, leading them to occupy more space. In addition, the fact that more polymer has been added to the scaffold composition must also be taken into consideration for the walls' thickness.

If we now look at a scaffold with a freeze-casting temperature of $-145°C$, it appears that the walls are slimmer by approx. 24% and both the micro- and macropores are narrower (resp. by 47% and 60%). This is understandable as a lower temperature prevents large solvent crystals from growing and instead favors rapid nucleation therefore leading to smaller micropores after lyophilization. However, it does not explain why the macropores are narrower (see below).

B.2) In order to understand the mechanisms involved during the scaffold formation, fast-phase contrast tomography freeze-casting experiments *in-operando* were carried out. This second type of experiments allowed us to assess the crystal growth under varying freezing conditions. Focusing first on the cold bottom plate, large clusters can be pointed out, similar to the ones previously noticed on fully made scaffolds (**Figure 3**). We can confirm here that they are due to nanoparticles partial sedimentation, as they are not soluble in DMC - unlike the polymer used - and therefore depend heavily on the suspension preparation. From that, care has been taken in preparing the solution to avoid excessive sedimentation.

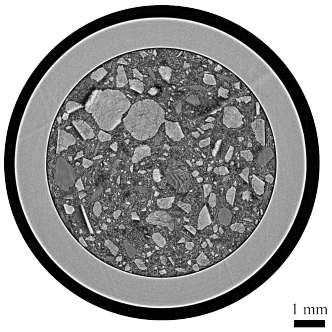

Figure 3. Cluster of sedimented nanoparticles (Bottom of suspension)

Following, a notable aspect that we could depict is the presence of micro-bubbles of dissolved gases (**Figure 4**). These air bubbles seem to appear as soon as the suspension came into

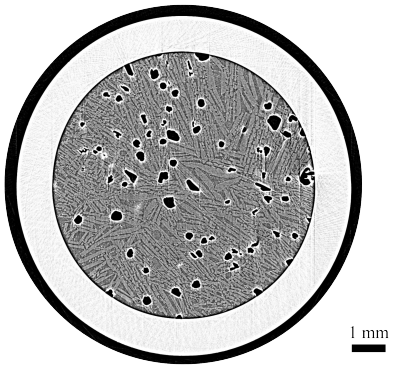

a) Micro-bubbles (black); lamellar crystallites (grey)

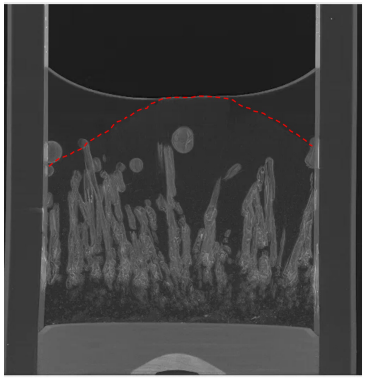

b) Micro-bubbles (clear grey); lamellar crystallites (dark grey) Roof-like solidification front in dotted red

Figure 4. Transversal (**a**) and longitudinal (**b**) cuts of a sample under-going freeze-casting, Vertical air channels forming macropores and solvent crystals forming micropores

contact with the cold bottom plate.

Preliminary tests with DMC show that freezing starts on the inner surface of the bubbles (air/DMC interface), meaning that crystals firstly grow inwards, where they require less energy. Furthermore, when examining samples containing nanoparticles and polymer in DMC, crystallite lamellar structures form between the air channels at temperatures of -5°C and below (knowing that the freezing temperature of pure DMC $T_{f,DMC} = 2 - 4°C$). When hollowed out, these solvent crystals are, as expected, responsible for the ladder-like microporosities and hybrid walls formation. In addition, we understood from this experiment that the macroporosity depicted during the experiments of static multi-resolution contrast phase tomography could be controlled and attributed to the aforementioned air bubbles' travels. It also appears that the walls are thicker around macropores when they first appear, which seems to confirm that these are preferential nucleation zones.

Image analysis reveal that the air bubbles follow different patterns of propagation. At first, bubbles seemingly move faster than crystals grow. During freeze-casting, the solidification front has a roof-like shape and the air bubbles reach the solid/liquid interface (**Figure 4.b**). As you move up the half-frozen/half-liquid suspension, the number of bubble channels decreases and their size increases, as some of them either coalesce or escape through the liquid/air interface. If the crystallization rate on either side of the bubble matches the moving bubble speed, meaning that crystal growth has caught up with the bubble, it creates an air channel up until the surface and the macropore is visible at the top of the scaffold. However, if the speed of crystallization exceeds that of the moving bubble, the crystals on either side of it meet and trap the bubble. Since cylindrical tubes form on the bubbles path, our understanding is that dissolved gas join the bubbles at the crystallization front. In this case, an underlying air channel is created which is not visible from the surface of the scaffold. Note that there might also be the possibility that micro-bubbles escape or still have some mobility through the intercrystalline spaces during crystallization and/or once the crystals have all formed.

To understand what could be responsible of narrower macropores when using a lower freezing temperature, as shown with the static multi-resolution contrast phase tomography, an experiment at $T_f = -25°C$ has been carried out. With these conditions, we distinguish the propagation of bubbles up until the surface of the meniscus. As explained above, it seems to mean that the crystallization rate almost immediately matches that of the moving bubbles therefore creating air channels. This phenomenon could explain why we keep a clear definition of the macropores even at the top of the scaffold and why they are narrower when freeze-casted at a colder temperature as they do not have sufficient time to coalesce.

The reasons for the presence of such a large quantity of bubbles have yet to be determined, but hypotheses are here and they need to be confronted with new ID19 experiments: 1- entrapping microbubbles when preparing suspensions, 2- microbubbles appearing from dissolved gas that are expelled from the solvent while it crystallizes at the freezing interface, 3- bubble nucleation sites on the particles aggregates and substrate such as the sample chamber walls, 4- Cavitation-like phenomenon due to particular pressure and hydrodynamical conditions inside the sample chamber during freeze-casting, etc.

PART C. Compression under axial load

Finally, with the goal of studying the mechanical behavior of the multi-porous scaffolds under load, a third approach was to use the ID19 TomoPress with custom-made plastic sample holders. Two scaffolds with different polymer/Np ratio were analyzed, 90/10 and 60/40. They were clamped

between the flat supports, which were larger than the diameter of the scaffolds, as to ensure the most uniform load possible on both sides of the structure. The experiments consisted in several cycles of compression up to the maximum capacity of the TomoPress (maximum longitudinal stroke of the motor on the y axis) followed by a 10-minute relaxation time. It should be noted that after relaxation, a full tomography scan was performed, adding about 25 minutes of relaxation time.

For both samples studied, we chose to represent the evolution of the force (N) applied with respect to the duration of the experiment, as well as stress (Pa) as a function of strain (%). 13 cycles of compression followed by relaxation were applied on the sample with a polymer/Np ratio of 60/40, while only 7 similar cycles were applied on the sample of a 90/10 polymer/Np ratio (due to lack of time to complete the 90/10 sample experiment during the last beam time). Therefore, only the first half on the two curves can be compared.

As **Figure 5** shows, they have similar behavior as they both seem to follow a non-linear model of elasticity. In that case, two Young's moduli can be noted for both samples, E_{low} and E_{high}, attesting to two different contributions. First hypotheses are that the E_{low} is related to the macropores partial collapse, while the micropores and then the polymer/nanoparticles response relates to E_{high}, as the scaffold may exhibit a stronger behavior thanks to its a cohesive and interconnected structure. Furthermore, the 90/10 polymer/Np ratio sample shows a steeper E_{high} ($E_{high,90/10}$ ~ 13011 Pa ; $E_{high,60/40}$ ~ 11307 Pa), which indicates that this sample has a more rigid structure. However, it seems that the yield stress is reached at a lower strain for this sample which tends to indicate that it is weaker than the other sample ($Yield_{stress,90/10}$ ~ 271200 Pa, at 32% ; $Yield_{stress,60/40}$ ~ 334220 Pa, at 54%). It therefore means that a composite scaffold with a higher nanoparticle mass ratio results in a stronger material than a scaffold consisting mainly of polymers.

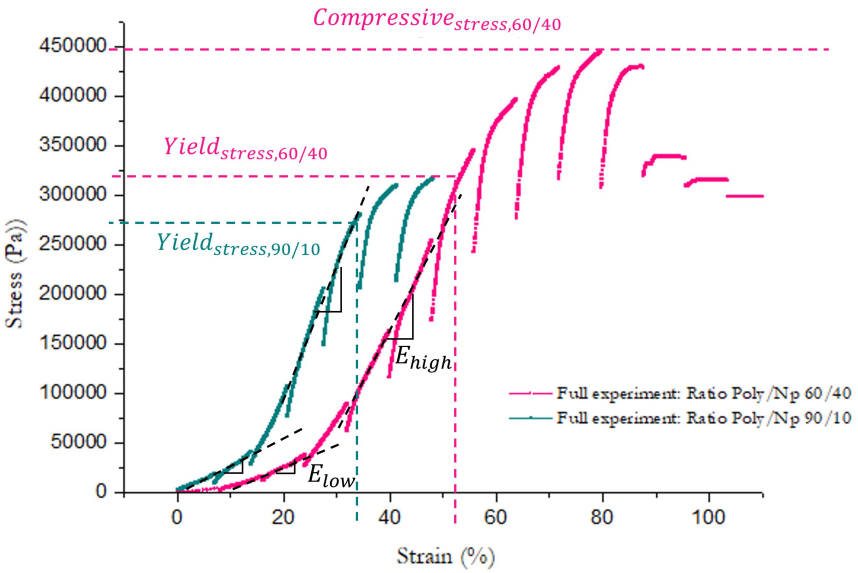

Figure 5. Stress (Pa) vs strain (%) curves for two samples with different polymer/Np ratio
Blue curve: 7 Compression cycles ; Pink curve: 14 Compressions cycles

Focusing now on the sample with a polymer/Np ratio of 60/40, the second half of the strain-stress curve seems to show that the material can distort plastically without breaking, for a strain of approximately 50 to 80%, meaning that the material is quite ductile.

However, after 90% of strain and a compressive stress of about 446 kPa, stress levels drop by 26%, typical of a strain-softening phenomenon. Material failure has begun, such as localized matrix cracking, leading to load redistribution and, in consequence, local strain-softening behavior, which is confirmed by the image analyses of the static tomography scans taken.

PART D. Conclusion and forthcoming work (a continuation proposal was deposited on the 11/09/2023).

The three-part experiments we conducted in our first ID19 synchrotron experiment enabled us to carry out a great number of feasibility tests, which in turn allowed us to obtain satisfactory results that highlight the need to control the formation of the air-channels from expelled gas during the freeze-casting process. All these results and the experiments newly proposed on ID19 (Proposal Ref. No 98816 deposited on the 11/09/2023), will be used for a scientific publication focusing on these essential issues to understand the freeze-casting mechanisms and the mechanical properties of the scaffolds.

Note that the multiscale porosity and particularly the tubular macropores are of great interest when they reach the external scaffold interfaces for blood and cell recolonization, provided they do not degrade mechanical properties too much.

Following our last beam-time experiment, our aim is now to gain a better understanding of the mechanisms involved in bubble nucleation, tubular pores formation and therefore of scaffolds' walls and multiscale porosity formation. With this purpose in mind, we aim to carry out freeze-casting *in-operando* X-ray tomography experiments with a new cryo sample chamber, with a seal designed to control pressure and dissolved gas in solution. In order to avoid or control bubble sizes, several suspension preparation methods will be studied: 1) degassed or gas-saturated suspensions, 2) freeze/thawn cycles, 3) different cold-bottom substrate surface states: atomically flat, mirror-polished metal caps, metal caps with controlled roughness.

Next, from these freeze-casted suspensions, hollowed scaffolds of different porosity will be obtained with a custom-made sublimation system coupled to the cryo sample chamber. Since the presence or absence of macropores has a significant impact on the intrinsic mechanical properties of the material, further study on the scaffolds formed in the conditions above will be carried out with a new commercial press available at ID19 (upgraded and now with a vertical compression instead of horizontal, easiest for compression/relaxation cycles). In addition to the destructive compression experiments which will be possible due to the higher maximum capacity of the new vertical press compared to the TomoPress used last time, fatigue testing will also be carried out in order to get as close as possible to the mechanical life of the scaffold once grafted into the jaw.